JOC The Journal of Organic Chemistry

Article

pubs.acs.org/joc

# Protonation Dependent Topological Dichotomy of Core Modified Hexaphyrins: Synthesis, Characterization, and Excited State Dynamics

Abhijit Mallick,[†,⊥] Juwon Oh,[‡,⊥] Marcin A. Majewski,[§] Marcin Stępień,*[,§] Dongho Kim,*[,‡] and Harapriya Rath*[,†]

[†]Department of Inorganic Chemistry, Indian Association for the Cultivation of Science, 2A/2B Raja S. C. Mullick Road, Jadavpur, Kolkata 700032, India

[‡]Department of Chemistry, Yonsei University, Seodaemun-gu, Seoul 120-749, Korea

[§]Wydział Chemii, Uniwersytet Wrocławski, ul. F. Joliot-Curie 14, 50-383 Wrocław, Poland

Supporting Information

**ABSTRACT:** Two hitherto unknown core modified hexaphyrin analogues have been synthesized and characterized where the conformational dynamics of these macrocycles in the free base form is achieved by the rotation of thienothiophene units. Further unique property of these macrocycles is the Hückel-Möbius topological switching. The thermodynamic equilibrium and kinetics of the interconversion leading to Hückel-Möbius switches have been triggered by external stimuli, such as protonation and/or temperature. We have provided a thorough solution-state spectroscopic characterization, solid-state structural evidence combined with in-depth theoretical calculations to investigate the crucial factors involved in such interconversion between Hückel and Möbius topologies for these hexaphyrins which will be useful in designing future new members to expanded porphyrin chemistry.

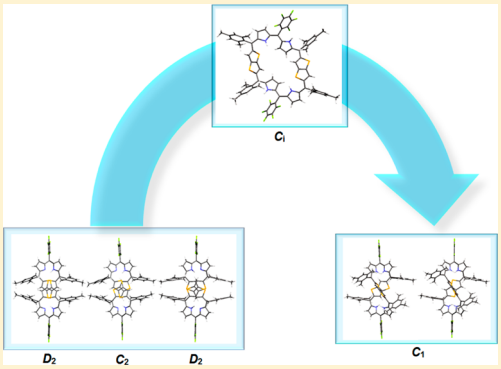


## INTRODUCTION

The rational design and synthesis of discrete and preorganized molecular systems with defined topology[1] are of interest due to their ion binding properties and conformational flexibility and allows one to explore uncharted frontiers in chemistry, biology, and other related areas. Recent years have witnessed a renaissance of interest from synthetic chemists in arriving at structurally nontrivial aromatic molecules with nonorientable (Möbius-band) $\pi$ surfaces.[2e] The molecular-orbital description of Möbius aromaticity predicts that singlet annulenes with $4n\pi$ electrons are aromatic systems in twisted conformations (with an odd number of half-twists) where the p orbitals lie on the surface of a Möbius strip, whereas singlet $[4n+2]$ Möbius molecules would be antiaromatic (the opposite of the Hückel rule).[2] Porphyrins and expanded porphyrins serve as a benchmark for extreme manifestations of aromaticity, antiaromaticity, pseudo aromaticity, and Möbius aromaticity.[3] Because of their large conformational flexibility, expanded porphyrins are the best platforms to adopt a Möbius topology since the large strain induced by the molecular twist is dissipated across the whole macrocyclic ring system. Thus, the initial finding of a Möbius porphyrinoid, A,D-di-*p*-benziporphyrin,[4a] was followed by subsequent reports on other Möbius aromatic porphyrinoids containing $[24]\pi$ or larger electronic conjugation pathways, which were stabilized and controlled by various factors, such as metal coordination, temperature, solvent effects, protonation equilibria, and peripheral substitution.[4] Much progress has been made in these endeavors but much remains unexplored. Hence there is an upsurge in demand for new synthetic expanded porphyrins for an in-depth study of aromaticity and $\pi$-conjugation. From literature reports, it is inferable that in sharp contrast to topographically flat fully conjugated expanded porphyrins, the propensity of figure-eight twisted geometries towards conformational fluxionality leads to topological switching from one conformation to another depending upon the protonation state and metalation.[5,6a] So far, multilevel switching behavior in a single macrocyclic entity has not been reported in all-pyrrole expanded porphyrins[4g] and their heterologues containing O, S, Se, or Te.[4h,i,6a] Experimental realization of new conformationally flexible expanded porphyrins might provide model systems for investigating the key issue of topologically controlled aromaticity switching.

## RESULTS AND DISCUSSION

Here we report the successful synthesis of two $[32]\pi$ heteroannulenes **6**-$H_2$ and **7**-$H_2$ (Scheme 1). These systems are (1.1.1.1.1.1) hexaphyrin analogues containing two thieno-[3,2-*b*]thiophene subunits (henceforth designated as TT) and

**Received:** October 25, 2016
**Published:** December 15, 2016





DOI: 10.1021/acs.joc.6b02576
J. Org. Chem. 2017, 82, 556−566

**Scheme 1. Synthesis of Macrocycles 6-$H_2$, 7-$H_2$**[a]

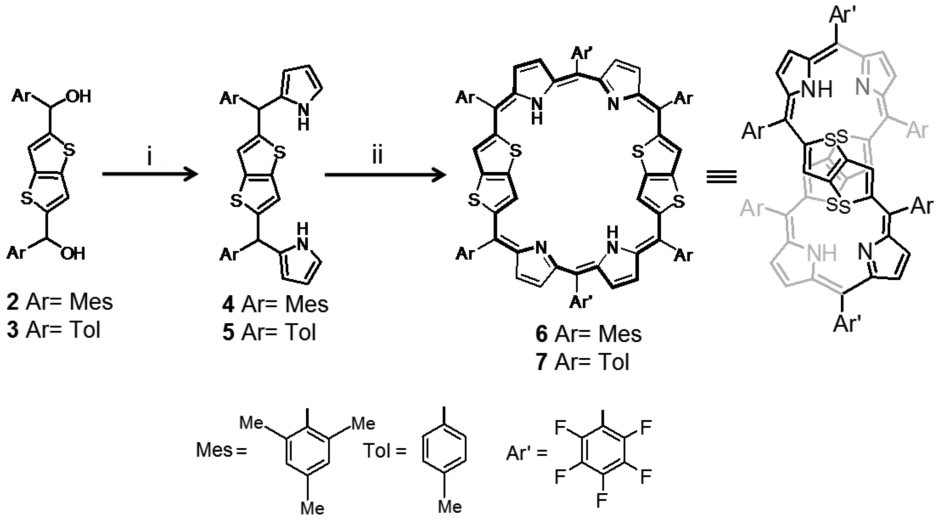


[a]Reagents and conditions: (i) pyrrole (50 equiv), trifluoro acetic acid (1 equiv); (ii) pentafluorobenzaldehyde, cat. PTSA, chloranil (2.5 equiv).

six *meso* bridges,[6] and differ in their *meso* substituents adjacent to the TT units (tolyl vs mesityl). The above design was chosen with the aim of creating conformationally flexible systems that might exhibit three distinct $\pi$-conjugation topologies depending upon the external stimuli. In an initial step leading to target macrocycles, thieno[3,2-*b*]thiophene **1** was synthesized following a literature report.[7] Because the steric bulk of the *meso*-aryl substituents play a decisive influence on the efficiency of macrocyclization,[8] two different tripyrrane analogues **4** and **5** were synthesized in two steps from **1** (Scheme S1).[9] The rational synthesis of macrocycles **6**-$H_2$ and 7-$H_2$ entailed a mild protic acid-catalyzed condensation of either **4** or **5** with pentafluorobenzaldehyde followed by oxidation with chloranil under reflux.[6] The addition of 0.1 equiv of *p*-toluene sulfonic acid gave the best yield for macrocycles **6**-$H_2$ and 7-$H_2$. Column chromatographic separation over basic alumina followed by repeated silica gel (200−400 mesh) chromatographic separation yielded the macrocycles **6**-$H_2$ and 7-$H_2$ in 6% and 8% yields, respectively, as dark green solids.

The new macrocycles were thoroughly characterized via spectroscopic and single crystal X-ray diffraction analyses. Macrocycles **6**-$H_2$ and 7-$H_2$ showed the parent ion peaks at *m*/*z* 1416.464 and 1304.156, respectively, under positive ionization in MALDI-TOF mass spectrometry (Figures S6, S7), thus confirming their elemental composition.

The expanded macrocycles **6**-$H_2$ and 7-$H_2$ were anticipated to show considerable conformational flexibility, as previously observed for various expanded porphyrinoids.[4−6] In both molecules, the structure bears a formal resemblance to A,D-di-*p*-benzihexaphyrin,[4a,b] because of the presence of two quasi-linear subunits (TT vs *p*-phenylene) in the macrocycle. On the basis of this similarity, a range of conformers were considered for the present ring systems, to facilitate further analysis. The lower symmetry of the rotatable TT fragments produces a larger number of distinct conformations that need to be considered, and we found it advantageous to classify these structures using the previously reported binary system.[3e] In particular, there are three distinct arrangements of the TT units in the figure-eight Hückel structure (denoted T2, because of the corresponding linking number Lk = 2).[3e,4c] In these arrangements, labeled ⟨0⟩, ⟨96⟩, and ⟨2145⟩ in Chart 1, the

**Chart 1. Conformations of 6-$H_2$ and 7-$H_2$ Discussed in the Article**[a]

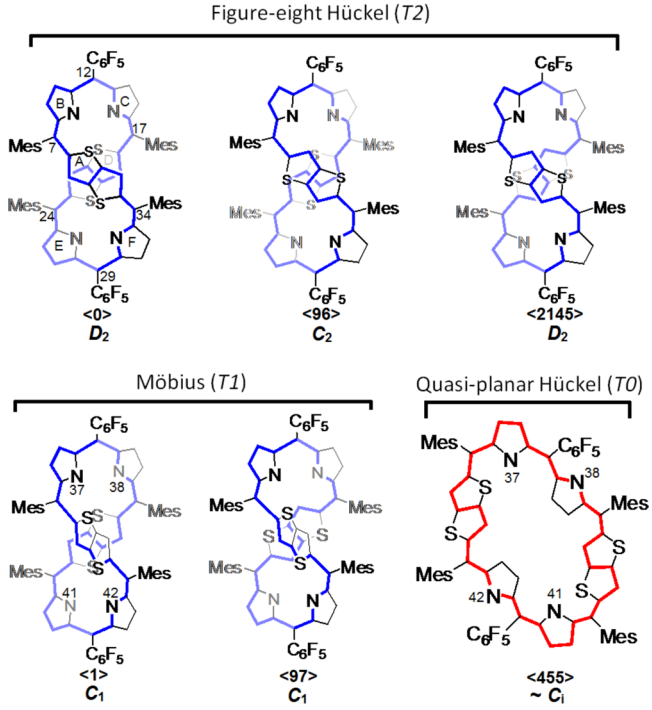


[a]$\pi$-Conjugation and NH protons pattern are not shown for clarity.

non-hydrogen atom framework can have the limiting point symmetry $D_2$, $C_2$, and $D_2$, respectively. Likewise two distinct Möbius T1 structures, ⟨1⟩ and ⟨97⟩, each of $C_1$ symmetry, can be considered. The symmetry of these conformations can be further lowered by protonation. In parallel with the spectroscopic work, we used DFT calculations to systematically analyze the geometries and relative energies for different protonation states of the above skeletal structures. Relevant results of this analysis are discussed below (for complete computational data, see the Supporting Information).

We have carried out thorough NMR studies in the free base as well as in the protonated state in order to investigate the



DOI: 10.1021/acs.joc.6b02576
J. Org. Chem. 2017, 82, 556−566

relationship between solution-state dynamic conformational changes and aromaticity in **6**-$H_2$ and **7**-$H_2$. Dynamic NMR studies support the premise that depending on the relative orientation of TT units at the crossing point, there are two T2 type conformers in the free base form of the macrocycle **6**-$H_2$ (Chart 1). The temperature-dependent behavior of the $^1$H NMR spectra of free base **6**-$H_2$ in $CD_2Cl_2$ indicates an effective $D_2$ symmetry, which is inferred from the equivalence of all mesityl groups and the nonequivalence of mesityl *o*-Me signals. This symmetry is consistent with a figure-eight Hückel structure that does not untwist on the NMR time scale, while undergoing a rapid NH proton transfer even at 175 K (Figure 1). Below 250 K, decoalescence of the peak at 18.12 ppm takes

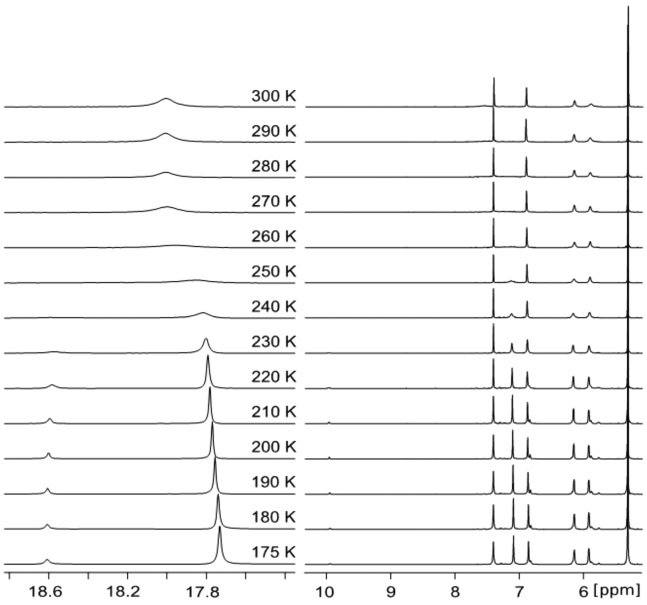


**Figure 1.** Selected regions of variable temperature $^1$H NMR spectra of **6**-$H_2$ ($CD_2Cl_2$, 600 MHz).

place, indicating two forms with different populations (the peaks at 17.75 and 18.61 ppm for major and minor species, respectively). The population of minor form decreases upon decreasing temperature (from 0.20 at 220 K to 0.15 at 175 K). The $^1$H NMR spectrum of the major conformer is similar to that at high-temperature spectrum and only a very weak ROE is observed between NH and TT protons at 190 K, representing the $D_2$ symmetry (Figure S30). These features are consistent with the orientation of TT units found in the ⟨0⟩ conformation of **6**-$H_2$ (Chart 1). This assignment is further supported by DFT calculations, which predict the lowest energy for the 37,41*H*-⟨0⟩-**6**-$H_2$ structure (Figure 2, Table 1). In the spectrum of the minor conformer, the peaks at 18.61 ppm (NH) and 9.96 ppm (TT) have equal integral intensities and show a strong dipolar contact in the ROESY spectrum (Figure S30). These features correspond to the $C_2$-symmetrical conformer ⟨96⟩, in which one of the TT subunits is rotated by 180° relative to its position in the ⟨0⟩ structure (Figure 2). The remaining signals of ⟨96⟩-**6**-$H_2$ were difficult to assign because of extensive overlap with the spectrum of major conformer (in particular, the other TT signal of ⟨96⟩-**6**-$H_2$ overlaps precisely with the TT line of ⟨0⟩-**6**-$H_2$). In accord with the experiment, DFT calculations predict 38,42*H*-⟨96⟩-**6**-$H_2$ as the second most stable structure (relative $\Delta G^0_{298}$ of 0.36 kcal/mol, Table 1).

The T2 topology of the $\pi$ system in the ⟨0⟩-**6**-$H_2$ and ⟨96⟩-**6**-$H_2$ conformers corresponds to two half-twists and an orientable surface. For a [32] annulenoid circuit, this topology is expected to produce a Hückel-antiaromatic $4n\pi$ system. The $^1$H chemical shifts are indicative of a moderate paratropic ring current. At 190 K in DCM-$d_2$, the paratropicity is demonstrated by the low-field positions of the inner NHs (17.76 and 18.60 ppm for ⟨0⟩-**6**-$H_2$ and ⟨96⟩-**6**-$H_2$), and of the unique TT proton of ⟨96⟩-**6**-$H_2$ residing in the cavity (9.96 ppm). Outer protons attached to the macrocycle are moderately affected by the ring current effect ($\beta$-CHs in the 5.8−6.2 ppm range). Finally in the Mes substituents, the endo *o*-Me groups (3.27 ppm in ⟨0⟩-**6**-$H_2$) are deshielded relative to those in 5-mesityldipyrrin (2.10 ppm), a feature previously shown to indicate paratropicity.[4b]

Importantly, the chemical shift pattern observed for the major form is in good quantitative agreement with GIAO shieldings calculated for the DFT model of 37,41*H*-⟨0⟩-**6**-$H_2$ at the KMLYP/6-31G(d,p) level of theory (Figure S31). In the present work, it was not possible to provide complete signal assignment for all species. The completeness of the assignment was limited in several cases by signal overlap and line broadening.

Variable-temperature $^1$H NMR measurements performed for **7**-$H_2$ revealed a similar conformational exchange between the ⟨0⟩ and ⟨96⟩ structures with moderate paratropic ring current. However, at room temperature, single *o*-Tol and *m*-Tol signals

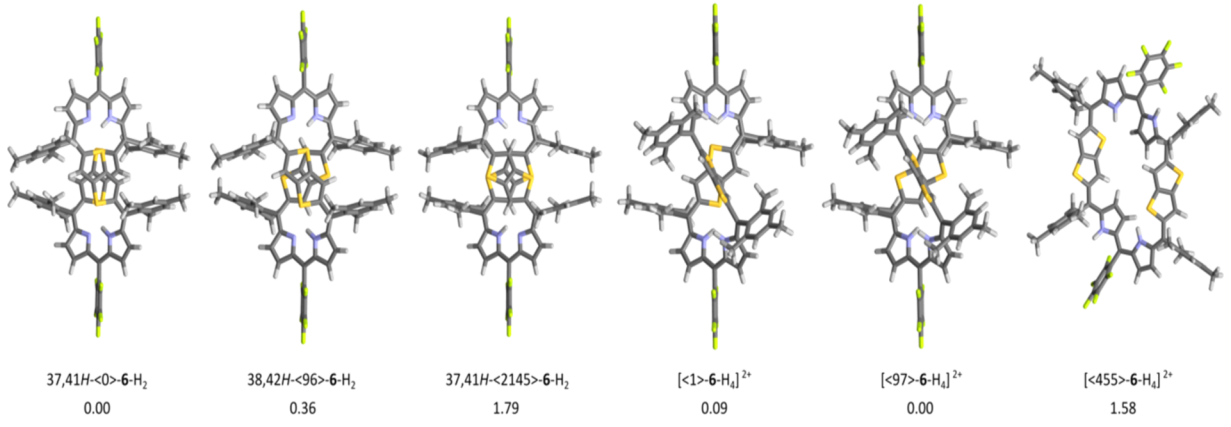


**Figure 2.** DFT-optimized geometries for selected conformers and tautomers of **6**-$H_2$ and [**6**-$H_4$]$^{2+}$. Gibbs free energies (PCM(DCM)/KMLYP/6-31G(d,p), kcal/mol, 298 K) are given relative to 37,41*H*-⟨0⟩-**6**-$H_2$ (for free bases), and relative to [⟨97⟩-**6**-$H_4$]$^{2+}$ (for dications).



DOI: 10.1021/acs.joc.6b02576
J. Org. Chem. 2017, 82, 556−566

**Table 1. Computational Data for 6-$H_2$ and Its Cations**

| name[a] | topology and protonation | SCF $E$[b] a.u. | $E_{rel}$[c] kcal/mol | ZPV[d] a.u. | min freq[e] $cm^{-1}$ | $\Delta G$[f] a.u. | $\Delta G_{rel}$[g] kcal/mol |
|---|---|---|---|---|---|---|---|
| neutral | | | | | | | |
| f_0000_37_41x | 37,41*H*-⟨0⟩ | −5959.772214 | **0.00** | 1.240085 | 10.48 | −5958.668453 | **0.00** |
| f_0000_37_42 | 37,42*H*-⟨0⟩ | −5959.755199 | **10.68** | 1.239838 | 10.24 | −5958.648461 | **12.55** |
| f_0001_37_41 | 37,41*H*-⟨1⟩ | −5959.757331 | **9.34** | 1.240305 | 8.31 | −5958.655465 | **8.15** |
| f_0001_38_41 | 38,41*H*-⟨0⟩ | −5959.750163 | **13.84** | 1.240189 | 6.72 | −5958.650246 | **11.43** |
| f_0096_37_41a | 37,41*H*-⟨96⟩ | −5959.769891 | **1.46** | 1.239991 | 10.60 | −5958.666208 | **1.41** |
| f_0096_37_42 | 37,42*H*-⟨96⟩ | −5959.753658 | **11.64** | 1.240012 | 8.84 | −5958.648597 | **12.46** |
| f_0096_38_41 | 38,41*H*-⟨96⟩ | −5959.757720 | **9.09** | 1.240223 | 9.86 | −5958.651024 | **10.94** |
| f_0096_38_42a | 38,42*H*-⟨96⟩ | −5959.769882 | **1.46** | 1.239894 | 7.42 | −5958.667879 | **0.36** |
| f_0097_37_41 | 37,41*H*-⟨97⟩ | −5959.754737 | **10.97** | 1.240038 | 3.49 | −5958.654846 | **8.54** |
| f_0097_37_42 | 37,42*H*-⟨97⟩ | −5959.757553 | **9.20** | 1.240140 | 7.21 | −5958.656100 | **7.75** |
| f_0097_38_41 | 38,41*H*-⟨97⟩ | −5959.753262 | **11.89** | 1.240297 | 7.39 | −5958.653315 | **9.50** |
| f_0097_38_42 | 38,42*H*-⟨97⟩ | −5959.757536 | **9.21** | 1.240427 | 7.86 | −5958.655437 | **8.17** |
| f_2145_37_41a | 37,41*H*-⟨2145⟩ | −5959.767270 | **3.10** | 1.239846 | 10.26 | −5958.665594 | **1.79** |
| f_2145_37_42 | 37,42*H*-⟨2145⟩ | −5959.753887 | **11.50** | 1.239799 | 5.80 | −5958.651880 | **10.40** |
| monocations | | | | | | | |
| f_0000 | 37,38,41*H*-⟨0⟩ | −5960.217048 | **0.00** | 1.254180 | 9.54 | −5959.096765 | **1.07** |
| f_0001_37_38_41 | 37,38,41*H*-⟨1⟩ | −5960.204840 | **7.66** | 1.254197 | 7.96 | −5959.088483 | **6.26** |
| f_0001_37_38_42 | 37,38,42*H*-⟨1⟩ | −5960.210743 | **3.96** | 1.254142 | 8.88 | −5959.094168 | **2.70** |
| f_0001_37_41_42 | 37,41,42*H*-⟨1⟩ | −5960.207898 | **5.74** | 1.254125 | 7.86 | −5959.091944 | **4.09** |
| f_0001_38_41_42 | 38,41,42*H*-⟨1⟩ | −5960.205744 | **7.09** | 1.254662 | 7.13 | −5959.088943 | **5.97** |
| f_0096_37_38_41 | 37,38,41*H*-⟨96⟩ | −5960.216025 | **0.64** | 1.254055 | 10.39 | −5959.098015 | **0.28** |
| f_0096_37_38_42 | 37,38,42*H*-⟨96⟩ | −5960.214118 | **1.84** | 1.253815 | 9.61 | −5959.096644 | **1.14** |
| f_0097_37_38_41 | 37,38,41*H*-⟨97⟩ | −5960.207275 | **6.13** | 1.254465 | 7.53 | −5959.090403 | **5.06** |
| f_0097_37_38_42 | 37,38,42*H*-⟨97⟩ | −5960.211155 | **3.70** | 1.254076 | 8.20 | −5959.095982 | **1.56** |
| f_0097_37_41_42 | 37,41,42*H*-⟨97⟩ | −5960.208800 | **5.18** | 1.253957 | 7.70 | −5959.093433 | **3.16** |
| f_0097_38_41_42 | 38,41,42*H*-⟨97⟩ | −5960.207787 | **5.81** | 1.254977 | 7.52 | −5959.091205 | **4.55** |
| f_2145 | 37,38,41*H*-⟨2145⟩ | −5960.212983 | **2.55** | 1.254012 | 8.82 | −5959.098463 | **0.00** |
| dications | | | | | | | |
| f_0000a | 37,38,41,42*H*-⟨0⟩ | −5960.648235 | **1.00** | 1.268539 | 7.85 | −5959.514542 | **1.30** |
| f_0001 | -⟨1⟩ | −5960.648777 | **0.66** | 1.268982 | 7.80 | −5959.516470 | **0.09** |
| f_0096a | -⟨96⟩ | −5960.623683 | **16.41** | 1.268563 | 10.86 | −5959.485483 | **19.53** |
| f_0097 | -⟨97⟩ | −5960.649831 | **0.00** | 1.269557 | 7.74 | −5959.516608 | **0.00** |
| f_0455 | -⟨455⟩ | −5960.647519 | **1.45** | 1.269560 | 8.58 | −5959.514093 | **1.58** |
| f_2145 | -⟨2145⟩ | −5960.645949 | **2.44** | 1.268316 | 6.82 | −5959.515649 | **0.60** |

[a]Data set name (.pdb files). [b]PCM(DCM)/KMLYP/6-31G(d,p) energies for optimized geometries. [c]Relative energies (separately for each protonation level). [d]Zero-point vibrational energy. [e]Lowest vibrational frequency. [f]Gibbs free energy. [g]Relative Gibbs free energies (separately for each protonation level).

were observed, corresponding to rapid exchange between the endo and exo positions in the Tol substituents (Figures S32, S33). This effect could be caused either by rapid rotation of the Tol groups or by inversion of the figure-eight twist of the macrocycle. The former explanation is in line with the reduced steric hindrance of the Tol groups in 7-$H_2$. As the rigidity of the macrocycle should not be significantly affected by the difference of substituents, the barrier to inversion is expected to be similar in **6**-$H_2$ and 7-$H_2$.

Single crystals suitable for X-ray diffraction were obtained by slow diffusion of methanol into toluene solutions of **6**-$H_2$ and 7-$H_2$. In the free-base form, macrocycles **6**-$H_2$ and 7-$H_2$ (Figures 3a and S58) were each observed to adopt the twisted Hückel ⟨0⟩ conformation prevalent in solution. In the structure of **6**-$H_2$, the dihedral angle for pyrrolic ring is 32.66°, for pyrrolenic ring is 24.57°, and for thienothiophene moiety is 11.24° with respect to the mean plane containing the six *meso* carbons. The distance between the centroids of the TT units in **6**-$H_2$ and 7-$H_2$ were 3.80 and 3.78 Å, respectively.

The acid−base chemistry of **6**-$H_2$ and 7-$H_2$ was initially investigated using spectrophotometric titrations with trifluoroacetic acid (TFAH) performed in 1,2-dichloroethane (DCE, Figure 4). The free base forms of **6**-$H_2$ and 7-$H_2$ showed major

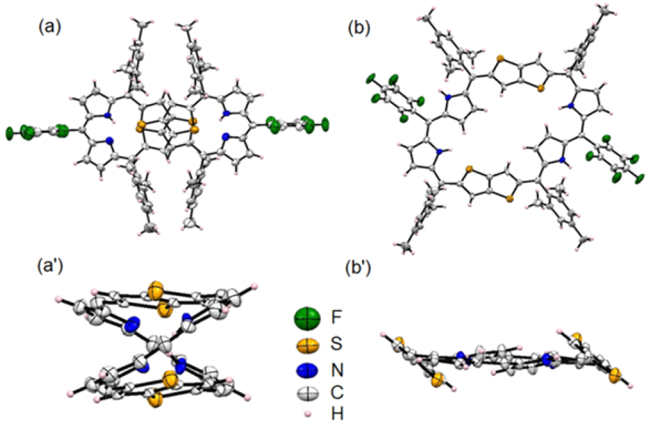


**Figure 3.** X-ray crystal structure of **6**-$H_2$ in (a) free base, (b) protonated form (a, b: plane view, a′, b′: side view). The thermal ellipsoids were scaled to the 50% probability level.



DOI: 10.1021/acs.joc.6b02576
J. Org. Chem. 2017, 82, 556−566

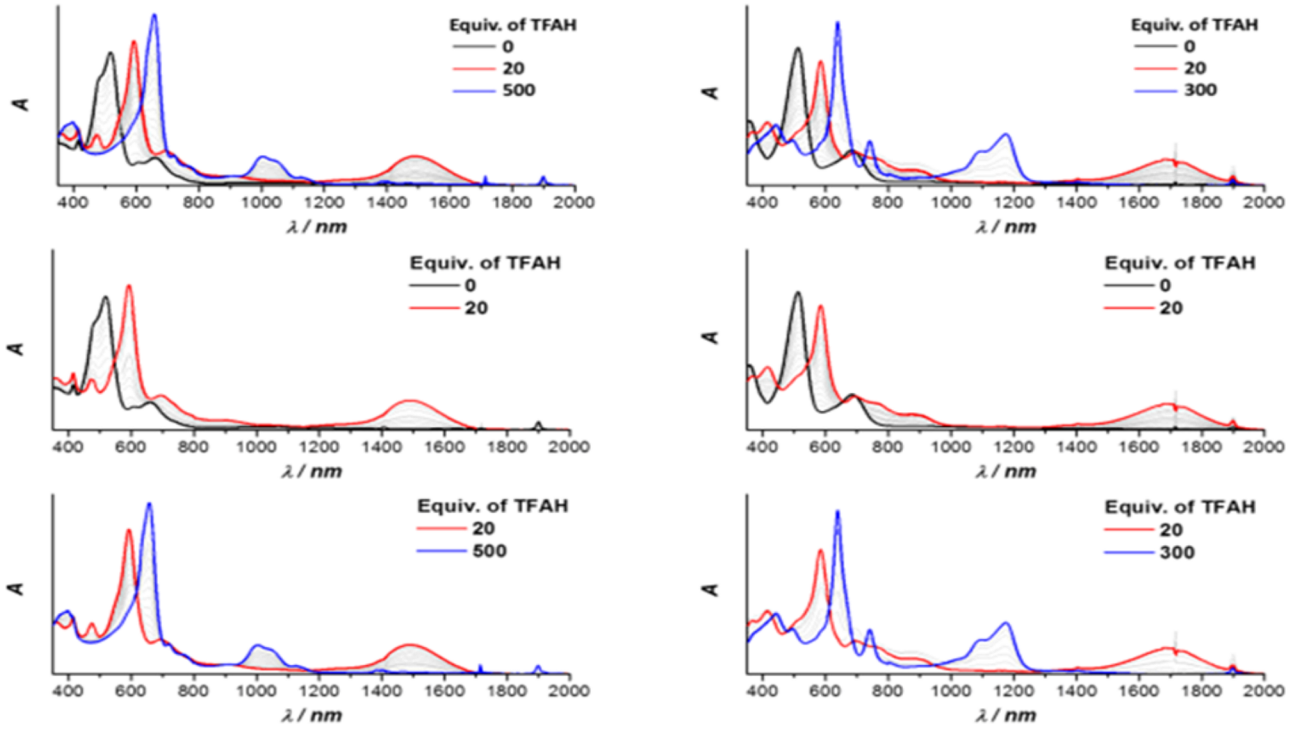


**Figure 4.** UV−vis-NIR absorption spectra of (a) **6**-$H_2$ and (b) 7-$H_2$ upon TFAH titration in 1,2-dichloroethane.

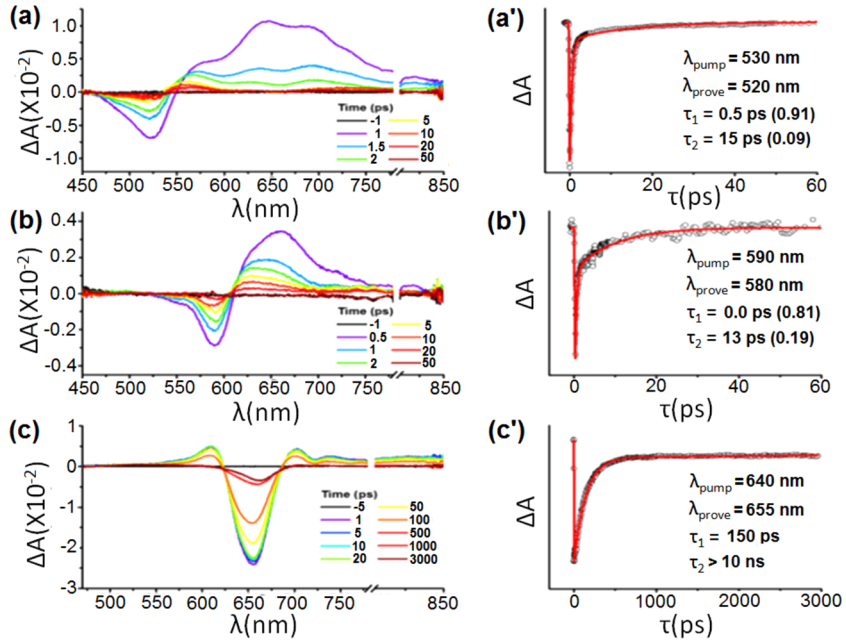


**Figure 5.** fs-Transient absorption spectra and decay profiles (inset) of **6**-$H_2$ with (a) 0, (b) 20, and (c) 500 equiv of TFAH in 1,2-dichloroethane.

absorption bands at 320, 517, and 658 nm for **6**-$H_2$ and at 357, 511, and 683 nm for 7-$H_2$, respectively, with absorption tailing over 1400 nm. The latter feature is characteristic of antiaromatic porphyrinoids, in line with the observation of T2-type conformers by $^1$H NMR spectroscopy. Both compounds turned out to be relatively weak bases and required a large excess of acid to undergo protonation. For each species, two well-defined protonation-related events with two isosbestic points were observed (Figure 4). For **6**-$H_2$, the two stepwise spectral changes exhibit isosbestic points at 547 and 617 nm whereas for 7-$H_2$, the two isosbestic points at 543 and 612 nm, respectively, upon the two stepwise spectral changes. In the first event, occurring at ca. 20 equiv of TFAH, a species with a broad, strongly NIR-shifted Q-like band was observed, with a maximum at 1500 and 1700 nm for **6**-$H_2$ and 7-$H_2$, respectively. For each system, the Soret-like maximum was also red-shifted from ca. 500 to 600 nm. The calculation results for protonated planar [⟨455⟩-**6**-$H_4$]$^{2+}$ and [⟨455⟩-7-$H_4$]$^{2+}$ with B3LYP/6-31g** show the forbidden transitions in the NIR region around 1600 nm (Table S1, Table S2). However, the experimental data show the conspicuous absorption bands at 1600−1800 nm. Such inconsistency can be attributed to the



DOI: 10.1021/acs.joc.6b02576
J. Org. Chem. 2017, 82, 556−566

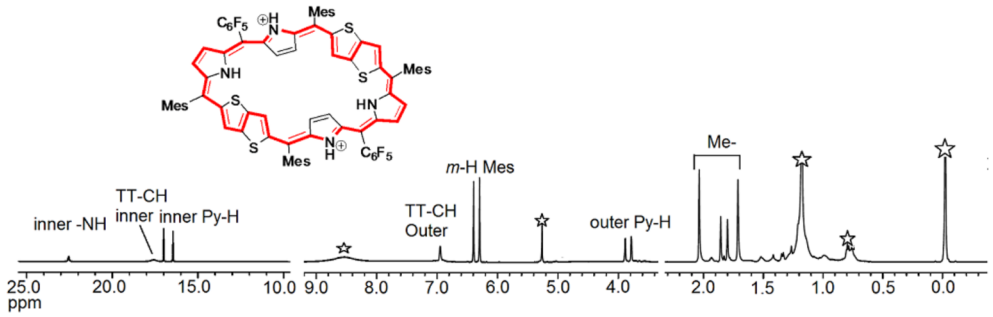


**Figure 6.** $^1$H NMR spectrum of protonated **6**-$H_4^{2+}$ in $CD_2Cl_2$ at 278 K.

hydrogen bond interactions between pyrrolic protons and TFA counteranions. Because 20 equiv of TFA are added for changing to $[\langle 455\rangle$-**6**-$H_4]^{2+}$ and $[\langle 455\rangle$-**7**-$H_4]^{2+}$, the hydrogen bond interaction may trigger distortion of planar structures and molecular complexes of $[\langle 455\rangle$-**6**-$H_4]^{2+}$ and $[\langle 455\rangle$-7-$H_4]^{2+}$ with TFA counteranions which can lead to the intensified lowest absorption bands in the NIR region. In the calculation based on the core macrocycle of $[\langle 455\rangle$-**6**-$H_4]^{2+}$ and $[\langle 455\rangle$-7-$H_4]^{2+}$, the forbidden transitions in the NIR region exhibited increased oscillator strengths when the TFA counteranions are calculated together (Figure S55). Thus, it is expected that the hydrogen bonding interactions and formation of molecular complexes lead to the enhanced absorption bands in 1600−1800 nm. An additional reaction with TFAH could be induced by using a very large excess of acid (300 to 500 equiv). The resulting absorption spectra were characterized by a major Q-like absorption in the 900−1200 nm range. In addition, fluorescence emission was observed in the NIR region at this stage of titration (Figure S26). The addition of triethylamine restored quantitatively the free base forms **6**-$H_2$ and 7-$H_2$ (Figure S27), indicating the reversibility of the entire acid-induced reaction sequence. Spectrophotometric TFAH titrations of **6**-$H_2$ and 7-$H_2$ in dichloromethane provided very similar results.

To gain deeper insight into the change of aromaticity by protonation, we investigated their excited state dynamics by fs-transient absorption (TA) measurements. In line with the changes in the absorption and $^1$H NMR spectra of **6**-$H_2$ and 7-$H_2$ by protonation, their TA spectra also showed drastic spectral changes (Figures 5 and S28). For free base **6**-$H_2$ and 7-$H_2$, the TA spectra showed the ground state bleaching (GSB) bands at 520 and 512 nm and the broad excited state absorption (ESA) bands over 550 and 535 nm for **6**-$H_2$ and 7-$H_2$, respectively. These TA spectra decayed with two time constants of 0.5 and 15 ps for **6**-$H_2$ and 0.4 and 15 ps for 7-$H_2$. The rapid and relatively slow decays in the order of fs and tens of ps suggest the presence of optically dark state typically, which are observed in the TA spectra of antiaromatic porphyrinoids.[10] In accordance with the absorption spectra of **6**-$H_2$ and 7-$H_2$ with 20 equiv of TFA, their TA spectra also showed red-shifted GSB and ESA bands. The decay of TA spectra were fitted with the two time constants of 0.2 and 13 ps for **6**-$H_4^{2+}$ and 0.1 and 14 ps for 7-$H_4^{2+}$. Compared to the free base forms, the acceleration of fast time constants are attributable to the more effective $\pi$-conjugation with enhanced antiaromaticity on the planar geometries. On the other hand, **6**-$H_2$ and 7-$H_2$ with 500 equiv of TFA displayed the typical features of aromatic porphyrinoids in the TA spectra containing strong GSB band with weak ESA bands.[10] Moreover, the excited state lifetimes were significantly increased. Along with their absorption spectra, these observations suggest the Möbius aromatic character of protonated **6**-$H_4^{2+}$ and 7-$H_4^{2+}$ under excess acid condition. Interestingly, in the comparative analysis between the TA spectra of protonated **6**-$H_4^{2+}$ and 7-$H_4^{2+}$ under excess acid condition, the clearer TA spectra and longer excited state lifetime were observed for protonated **6**-$H_4^{2+}$. These differences can also be explained on the basis that the mesityl substituents of **6**-$H_2$ induce more rigidity compared to tolyl substituents of 7-$H_2$.

To elucidate the conformational changes attendant upon TFAH addition, $^1$H NMR spectra were recorded for **6**-$H_2$ under diverse sets of conditions involving changes of solvent (DCM-$d_2$, 1,2-DCE-$d_4$, acetone-$d_6$), acid concentration (up to ca. 1000 equiv), and temperature. Upon addition of excess trifluoroacetic acid (19 equiv, as 1% solution in DCM-$d_2$, room temperature), dramatic changes in the spectral pattern were observed, consistent with the formation of a dicationic species, **6**-$H_4^{2+}$ (Figures S35−S38).

The occurrence of ring inversion was inferred from the observation of two sets of correlations in 2D COSY spectra (Figure S37), one between a pair of doublets at 16.3−16.9 ppm and another between a pair of doublets at 3.7−3.8 ppm, both corresponding to $\beta$-CH protons of pyrrole rings. The distinction between the inverted pyrrole and noninverted pyrrole ring $\beta$-CH protons was further based on 2D NOESY spectra (Figure S38). The $^1$H NMR spectrum of **6**-$H_4^{2+}$ at 278 K (Figure 6) showed an NH signal at 22.65 ppm, identified by $D_2O$ exchange experiments (Figure S39), which is assumed to correspond to the noninverted pyrroles. The NH signal of the inverted pyrrole ring is likely broadened by hydrogen bonding and could not be located in the spectrum. The spatial proximity between *o*-methyl protons of one set of Mes groups (2.04 ppm) with adjacent $\beta$-CH protons of the noninverted pyrrole ring (3.78 ppm) and outer $\beta$-CH proton of the thiophene ring (6.94 ppm) produced the expected dipolar contacts in the NOESY spectrum, providing unequivocal assignment of the three signals. Consequently, the signals at 16.37 and 16.90 ppm were assigned to inner $\beta$-CH protons of the inverted pyrrole ring. The peak at 15.31 ppm, which showed no correlation with any other peak in either COSY or NOESY spectra, was proposed to correspond to the inner $\beta$-CH proton of thiophene. The two distinct singlets at 6.29 and 6.39 ppm have been assigned to the *m*-CH protons of two different *meso*-mesityl rings based on correlations that each signal shows to *o*-methyl and *p*-methyl signals in the 2D COSY spectra (Figure S37). The observation of inner NH signals at 22.65 ppm is a diagnostic feature of a paratropic ring current, which is further manifested in the respectively upfield and downfield shifts of other inner and outer protons attached to the macrocycle. These spectral features could be rationalized in terms of double


DOI: 10.1021/acs.joc.6b02576
J. Org. Chem. 2017, 82, 556−566

pyrrole ring inversion, leading to a quasi-planar conformer $[\langle 455\rangle$-**6**-$H_4]^{2+}$ (Chart 1, Figure 2). An exactly similar NMR spectral pattern has been observed upon addition of excess trifluoroacetic acid (19 equiv, as 1% solution in $CDCl_3$, room temperature), for **7**-$H_2$ consistent with the formation of a dicationic species, **7**-$H_4^{2+}$ (Figures S40−S42). Thus, a quasi-planar conformer $[\langle 455\rangle$-**7**-$H_4]^{2+}$ with two pyrrole ring inversion can also be envisaged for **7**-$H_4^{2+}$.

Further support for the feasibility of the $\langle 455\rangle$ conformer was obtained from an X-ray crystallographic analysis. Single crystals of a trifluoroacetate salt $[$**6**-$H_4][CF_3CO_2]_2\cdot[CF_3COOH]_4$ were obtained by diffusion of hexane into the $CF_3COOH$/dichloromethane solution of **6**-$H_2$. The solid-state geometry of **6**-$H_4^{2+}$ was quasi-planar (Figure 3b). There is one centrosymmetric dication in the unit cell, and it is hydrogen-bonded to two dihydrogen tris(trifluoroacetate) assemblies via the NH hydrogens of inverted pyrroles (Figure S56). The inverted pyrrole rings deviated more strongly from the mean plane containing the six *meso* carbons compared to the noninverted pyrrole rings (13.32° vs 8.56°). The largest tilt was however exhibited by the TT units (38.28°).

Interestingly, when a smaller amount of acid (ca. 1 equiv) is added to the DCM-$d_2$ solution of **6**-$H_2$, the $^1$H NMR spectrum becomes broadened but the positions of peaks remain virtually unaltered. Likewise, the initial changes of optical absorption spectra are insignificant, indicating that the initial figure-eight conformers **6**-$H_2$ are relatively weak bases. The formation of the $\langle 455\rangle$ dication requires a double pyrrole ring inversion and is apparently not instantaneous. The rate of ring inversion is accelerated by temperature and by the increasing acid concentration. When a solution of **6**-$H_2$ in DCM-$d_2$ was treated with ca. 35 equiv of TFAH and immediately cooled down to 210 K, a spectrum with effective $D_2$ symmetry was observed (Figure S43), which was clearly distinct from the spectrum of the $\langle 455\rangle$ dication. Conversion of the $D_2$ intermediate into the $\langle 455\rangle$ species was however observed when the sample was left to stand at room temperature.

The transient low-temperature spectrum showed moderate diatropic characteristics, which could be inferred from $^1$H shift values, and was thus assumed to correspond to Möbius-type T1 conformations ($\langle 1\rangle$ and $\langle 97\rangle$) in the limit of fast rotation of TT units. Specifically, the $\beta$-CH signals were shifted to 7.30 and 7.19 ppm, whereas a broadened peak, assigned as the TT signal, was found at 5.23 ppm. The latter shift, which is dynamically averaged over four nonequivalent sites that are present in stationary T1 structures, is consistent with the upfield relocation previously observed in the symmetry-averaged spectra of A,D-di-*p*-benziporphyrin.[4a,b] The Me-*o*-Mes signals in the $\langle 1/97\rangle$ species resonate at 2.89 and 0.40 ppm. While the available 2D NMR data (Figure S44) were insufficient to assign these two peaks, they are expected to correspond respectively to exo and endo positions, in line with the previously established shielding effects in A,D-di-*p*-benziporphyrin.[4a,b]

It should be noted that the protonation status of the transient species discussed above could not be determined at 210 K, but the formation of the dication is considered probable in the presence of a large acid excess. Below 210 K, the spectrum underwent decoalescence, consistent with the expected lower symmetries of stationary conformers, but significant line broadening precluded more detailed analysis of these complex spectral patterns. Stepwise low-temperature titration of **6**-$H_2$ with TFA produced intermediate spectral patterns of considerable complexity, and apparently lower symmetry. DFT-derived $\Delta G^0_{298}$ energies calculated for $[\langle 1\rangle$-**6**-$H_4]^{2+}$ and $[\langle 97\rangle$-**6**-$H_4]^{2+}$ were very similar (0.09 and 0.00 kcal/mol), indicating that the two conformers may coexist in solution at experimentally available temperatures. The energy of the quasi-planar $\langle 455\rangle$ system was slightly higher (1.58 kcal/mol). It should be noted, however, that in these calculations, hydrogen-bonded interactions with carboxylate anions and acid molecules were not included. Such interactions are expected to be important, especially at high acid concentrations, and have been shown previously to affect the conformational dynamics of expanded porphyrins.[4] Overall, the above experimental and theoretical data indicate that the T2-type free base of **6**-$H_2$ does not undergo ring inversion when protonated at low temperatures, and the limiting species generated under excess acid conditions is most likely a mixture of Möbius aromatic $[\langle 1\rangle$-**6**-$H_4]^{2+}$ and $[\langle 97\rangle$-**6**-$H_4]^{2+}$ dications.

$^1$H NMR spectra of $[$**6**-$H_4]^{2+}$ obtained in the presence of a very large excess of TFAH (more than 300 equiv) were found to reveal an effective $D_2$ symmetry and chemical shifts consistent with a diatropic ring current. Such a spectrum was observed in 1,2-DCE-$d_4$ at 273 K (Figure S45), when the sample of **6**-$H_2$ was treated with ca. 120 equiv of TFAH. When the amount of acid was gradually increased to ca. 1000 equiv the spectrum became sharper. The $^1$H shifts underwent only minor changes of chemical shifts, likely resulting from interactions with excess TFAH (final values: $\beta$-H 7.21 and 7.15 ppm, TT 5.99 ppm, NH 5.84 ppm). A sharp, high symmetry spectrum, with similar shifts ($\beta$-H 7.53 and 7.09 ppm, TT 6.37 ppm, NH not observed, *o*-Mes 2.85, 0.60, *m*-Mes 7.20, 6.62, *p*-Mes 2.23 ppm, Figure S47) was also observed in acetone-$d_6$ in the presence of TFAH (ca. 20% v/v). The associated electronic absorption spectrum was however different in comparison with the DCE experiment: while the position of the Soret band was preserved, the Q bands were observed in the 800−1000 nm range in the acetone solution (Figure S24). In acetone-$d_6$, exchange cross-peaks between endo and exo positions of the Mes group were observed for $[$**6**-$H_4]^{2+}$ in the ROESY spectrum (Figure S49), indicating a slow untwisting of the figure-eight structure. On lowering the temperature, gradual line broadening was observed, but the symmetry of the spectrum remained unchanged down to 170 K.

The $^1$H NMR spectrum of $[$**6**-$H_4]^{2+}$ observed in the presence of a large acid excess is very similar to that observed for the transient $\langle 1/97\rangle$ conformer generated at low temperature, and it is tempting to suggest that the conformation of the high excess acid species might in fact be the same. While such an interpretation is most likely, it should be noticed that the $^1$H NMR spectrum is in all cases being observed in the limit of fast exchange, and exact structures of these conformers are not accessible. In particular, the conformational changes induced at different acid concentrations may involve not only rotations of TT units (which generate the $\langle 0, 1, 96, 97, 2145\rangle$ conformers, and are sufficient to induce topology switching) but also additional twists of the macrocycle near pyrrole rings. As long as such a twist does not lead to a complete inversion of the figure-eight structure, a $D_2$ symmetric spectrum is expected in the fast exchange limit. Nevertheless, the symmetry-averaged $^1$H shifts observed at high acid concentrations are consistent with a moderately diatropic structure, as indicated by the downfield positions of $\beta$-H signals ($\delta$ > 7 ppm), and the unusually upfield position of the TT signal. The latter change is similar to that observed for the *p*-phenylene signal in the $^1$H NMR spectrum of A,D-di-*p*-benzihexaphyrin,[4a] and may thus


DOI: 10.1021/acs.joc.6b02576
J. Org. Chem. 2017, 82, 556−566

indicate a Möbius-type T1 conformer. In line with the latter conjecture, the $^1$H NMR shifts of $[\mathbf{6}\text{-}H_4]^{2+}$ measured in acetone-$d_6$ are in a semiquantitative yet still remarkably good agreement with the $D_2$-averaged GIAO shieldings calculated for the lowest-energy dication $\langle 97\rangle$-$[\mathbf{6}\text{-}H_4]^{2+}$ (Figure S50). In particular, the calculation correctly reproduces the downfield relocations of $\beta$-H signals and the upfield position of TT (7.02 ppm), relative to the T2 free base.

The conformational change observed at different acid concentrations is most likely promoted by association of TFA anions and TFAH molecules to the $[\mathbf{6}\text{-}H_4]^{2+}$, in analogy to the behavior observed for A,D-di-*p*-benziporphyrin in the presence of dichloroacetic acid.[4b] However, since the present system is observed only in the fast exchange limit, the exchange between bulk and associated acid molecules and anions results in the complete loss of any structural information related to the acid binding and symmetry averaging of the $^1$H NMR spectral pattern of $[\mathbf{6}\text{-}H_4]^{2+}$.

In different solvents and at different acid concentrations, the stationary geometries are likely to differ because of hydrogen-bonded interactions with TFAH molecules. Acid association in solution was previously demonstrated for A,D-di-*p*-benzihexaphyrin[4b] as well as for other porphyrinoid systems.[4] Association with TFAH is expected to be significantly stronger in DCE (and DCM) than in acetone, because of the higher polarity of the latter solvent, and may explain why the absorption spectrum of $[\mathbf{6}\text{-}H_4]^{2+}$ in acetone is different.

The conformational behavior of $\mathbf{6}\text{-}H_2$ in DCE at various acid concentrations is summarized in Scheme 2. When the

**Scheme 2. Acid−Base and Conformational Behavior of $\mathbf{6}\text{-}H_2$ in 1, 2- DCE**

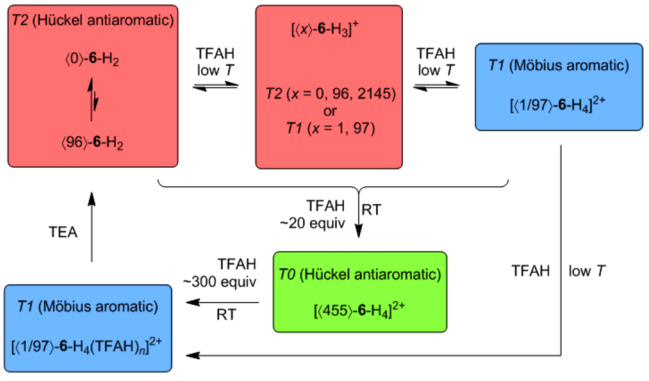


protonation is performed at low temperatures (below ca. 273 K with rapid acid addition), the figure-eight twist of the macrocycle is preserved, and the system goes from the T2 free base structure (the $\langle 0/96\rangle$ equilibrium mixture) via an unspecified mixture of T2 and T1 conformations at the monocation level to the predominantly T1-type dication. The spectral symmetry of this species and its diatropic character are retained over a wide range of acid concentrations, implying that the conformation is preserved. However, extensive association with acid molecules is indirectly observed above 100 equiv of TFAH. When $\mathbf{6}\text{-}H_2$ is titrated at room temperature, the dication undergoes double pyrrole inversion in the initial titration phase, to yield the quasi-planar $[\langle 455\rangle$-$\mathbf{6}\text{-}H_4]^{2+}$ species. The latter conformer is stable up to ca. 20 equiv of TFAH, but it reverts to the figure-eight Möbius structure $[\langle 1/97\rangle$-$\mathbf{6}\text{-}H_4]^{2+}$, when more acid is added. A qualitatively similar behavior was observed for $\mathbf{7}\text{-}H_2$ upon titration with TFAH in dichloromethane-$d_2$ (Figure S51), but the system was less amenable to 2D spectral analysis (Figure S53). A spectrum clearly corresponding to the T2 conformer $[\langle 455\rangle$-$\mathbf{7}\text{-}H_4]^{2+}$ was observed at intermediate acid concentrations. In the presence of a large excess of TFAH, the appearance of the spectrum indicated the presence of multiple forms. The major species observed at 263−243 K (Figure S52) could however be identified as a $D_2$-symmetric diatropic structure $\beta$-pyrroles: 8.06, 7.96 ppm, TT 5.87 ppm, Figure S54). In particular, this species features a single set of signals corresponding to a slowly rotating Tol substituent (*ortho* 8.13, 6.21 ppm, *meta* 7.28, 7.11 ppm, *p*-Me 2.33 ppm). This result is again consistent with the prevalence of a Möbius species at high acid concentrations proposed above for $\mathbf{7}\text{-}H_2$ on the basis of TA spectroscopy.

## CONCLUSION

In conclusion, the present article provides many insights into the conformational behavior of a highly twisted fused [32] heteroannulene associated with various topologies. Excellent agreement between the theoretically determined properties and the experimental spectroscopic measurements are key to the evidence of weak twisted-Hückel antiaromatic, strongly Hückel antiaromatic, and Möbius aromatic states, respectively, upon stepwise protonation. Our results are in accordance with the fact that protonation disrupts intramolecular H-bonding thereby leading to topological dichotomy in order for the macrocycle to gain aromatic stabilization energy. Further development of dynamic heteroannulenes is currently under progress in our laboratory.

## EXPERIMENTAL SECTION

**Materials and Methods.** Electronic absorption spectra were measured with a UV−vis-NIR spectrophotometer, and variable temperature UV−vis-NIR were carried out in cryostat. $^1$H, and $^{13}$C NMR spectra were recorded on a spectrometer (operating as 600.17 MHz for $^1$H and 150.91 MHz for $^{13}$C) using the residual solvents as the internal references for $^1$H [($CHCl_3$ ($\delta$ = 7.26 ppm), $CH_2Cl_2$ ($\delta$ = 5.32 ppm), acetone ($\delta$ = 2.04 ppm), and DCE ($\delta$ = 3.72 ppm)].

High-resolution electrospray ionization time-of-flight mass spectroscopy (HR-ESI-TOF MS) was conducted by using the positive mode for an acetonitrile solution of samples. All solvents and chemicals were of reagent grade quality, obtained commercially, and used without further purification except as noted. For spectral measurements, anhydrous dichloromethane was obtained by refluxing and distillation over $CaH_2$. Dry THF was obtained by refluxing and distillation over pressed Sodium metal. Thin layer chromatography (TLC) was carried out on alumina sheets coated with silica gel 60 $F_{254}$ and gravity column chromatography were performed using Silica Gel 230−400 mesh.

**X-ray Structure Determination.** Crystallographic data were collected at 100 K by using graphite-monochromated Mo K$\alpha$ ($\lambda$ = 0.71073 Å). The structures were solved by SHELX-2014 using SHELXTL suite of program. The final refinement of the structure was carried out using least-squares method on $F^2$ using SHELXL-2014. The final refinement of the solved structure converged at the R value of 0.0856 ($I > 2\sigma(I)$) for free base form of $\mathbf{6}\text{-}H_2$ and R value of 0.0737 ($I > 2\sigma(I)$) for protonated form of $\mathbf{6}\text{-}H_4^{2+}$ and R value of 0.0677 ($I > 2\sigma(I)$) for free base $\mathbf{7}\text{-}H_2$. All non-hydrogen atoms were refined anisotropically. All the hydrogen atoms were located from difference Fourier maps. For protonated $\mathbf{6}\text{-}H_4^{2+}$, ALERT 2A, 2B arises from potentially disordered solvent molecules. We tried to fix by using PART command, however atomic displacement values did not reduce.

**Femtosecond Transient Absorption Measurements.** The femtosecond transient absorption (fs-TA) spectra were measured with a spectrometer consisting of two independently tunable


DOI: 10.1021/acs.joc.6b02576
J. Org. Chem. 2017, 82, 556−566

homemade optical parametric amplifiers (OPSs) pumped by a regeneratively amplified Ti:sapphire laser system operating at a repetition rate of 1 kHz and an optical detection system.

**Theoretical Calculation.** Density functional theory (DFT) calculations were performed using Gaussian 09.[11] DFT geometry optimizations were carried out in unconstrained $C_1$ symmetry, using molecular mechanics or semiempirical models as starting geometries. DFT geometries were refined to meet standard convergence criteria, and the existence of a local minimum was verified by a normal-mode frequency calculation. DFT calculations were performed using the KMLYP functional[12] and the 6-31G (d, p) basis set. PCM solvation (dichloromethane parametrization) was included in all calculations. NMR chemical shifts were calculated using the GIAO/KMLYP/6-31G (d, p) level of theory. The absolute shielding of TMS calculated at the KMLYP level of theory was 31.946 ppm. Electronic absorption spectra were calculated using time-dependent DFT in the Tamm−Dancoff approximation, using the B3LYP functional and dichloromethane solvation. Up to 50 transitions were calculated, providing full coverage of the NIR and visible regions.

## SYNTHESIS

**Thieno[3,2-*b*]thiophene (1).**

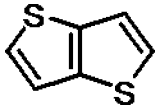

This was synthesized as reported in literature. Yield: 60%. Colorless crystalline solid. mp 53−58 °C. $^1$H NMR (300 MHz, $CDCl_3$): $\delta$ [ppm]: 7.26−7.28 (d, 2H, J = 4.8 Hz); 7.38−7.40 (d, 2H, J = 5 Hz). $^{13}$C NMR (75 MHz, $CDCl_3$, 300 K, $\delta$ [ppm]): 119.6, 127.6, 139.7. HR-ESI-TOF MS ($m/z$): Found 162.9631[M+Na]$^+$ (Calcd 162.9647 for $C_6H_4S_2Na^+$). Anal. Calcd for $C_6H_4S_2$: C, 51.39; H, 2.88. Found: C, 51.41; H, 2.90.

**(2,5-Bis (mesitylhydroxymethyl)-thieno[3, 2-*b*]thiophene (2).**

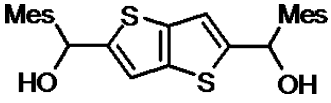

To a 250 mL round-bottomed flask equipped with a magnetic bar, thieno[3, 2-*b*]thiophene **5** (1 g, 7.13 mmol) was placed followed by dry THF (40 mL). The reaction mixture was stirred under inert atmosphere. *N*,*N*,*N*′,*N*′-Tetramethyl ethylenediamine (3.2 mL, 0.021 mol) was added followed by stirring for half an hour at room temperature. Afterward *n*-BuLi in hexane (1.6 M) (13.04 mL, 0.021 mol) was added through rubber septa dropwise, yellow turbidity started forming. The reaction mixture was stirred at room temperature for 2 h and then heated to 66 °C for 1 h. The reaction mixture was brought room temperature after which it was brought to ice cold temperature. At ice cold temperature, Mesitaldehyde (2.62 mL, 0.017 mol) in dry THF (40 mL) was then added dropwise to the reaction mixture, the reaction mixture was stirred for 2 h. The reaction mixture was quenched by saturated $NH_4Cl$ (aq) solution, product was extracted by diethyl ether, dried over $Na_2SO_4$. The crude product was precipitated out by hexane and purified by silica gel column chromatography using ethyl acetate−hexane (1:4) solution. The solvent was evaporated and light yellow solid was obtained. Yield 2.09 g (67%). Mp 156 °C. $^1$H NMR (500 MHz, $CDCl_3$, 300 K, $\delta$ [ppm]): 2.28 (s, 6H); 2.33 (s, 12H); 6.46 (s, 2H); 6.71 (s, 2H); 6.87 (s, 4H); $^{13}$CNMR (125 MHz, $CDCl_3$, 300 K, $\delta$ [ppm]): 20.6, 29.8, 69.8, 116.4, 130.2, 135.3, 137.0, 137.9, 138.3, 148.8. HR-ESI-TOF MS ($m/z$): Found 459.1430[M+Na]$^+$ (Calcd 459.1423 for [$C_{26}H_{28}O_2S_2Na$]$^+$). Anal. Calcd for $C_{26}H_{28}O_2S_2$: C, 71.52; H, 6.46. Found: C, 71.50; H, 6.44.

**(2,5-Bis(tolylhydroxymethyl)-thieno[3,2-*b*]thiophene (3).**

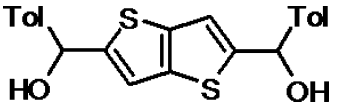

To a 250 mL round-bottomed flask equipped with a magnetic bar, thieno[3,2-*b*]thiophene **5** (1 g, 7.13 mmol) was placed followed by dry THF (40 mL). The reaction mixture was stirred under inert atmosphere. *N*,*N*,*N*′,*N*′-Tetramethyl ethylenediamine (3.2 mL, 0.021 mol) was added followed by stirring for half an hour at room temperature. Afterward *n*-BuLi in hexane (1.6 M) (13.04 mL, 0.021 mol) was added through rubber septa dropwise, yellow turbidity started forming. The reaction mixture was stirred at room temperature for 2 h and then heated to 66 °C for 1 h. The reaction mixture was brought room temperature after which it was brought to ice cold temperature. At ice cold temperature, *p*-tolylaldehyde (2 mL, 0.017 mol) in dry THF (40 mL) was then added dropwise to the reaction mixture, the reaction mixture was stirred for 2 h. The reaction mixture was quenched by saturated $NH_4Cl$ (aq) solution, product was extracted by diethyl ether, dried over $Na_2SO_4$. The crude product was precipitated out by hexane and purified by silica gel column chromatography using ethyl acetate−hexane (1:4) solution. The solvent was evaporated and light yellow solid was obtained. Yield 2.09 g (77.5%). mp 135 °C. $^1$H NMR (500 MHz, $CDCl_3$, 300 K, $\delta$ [ppm]): 2.35 (s, 6H); 6.02 (s, 2H); 6.97 (s, 2H); 7.17−7.18 (d, 4H, $^3$J = 8 Hz); 7.33−7.34 (d, 4H, $^3$J = 8 Hz). $^{13}$CNMR (125 MHz, $CDCl_3$, 300 K, $\delta$ [ppm]): 29.8, 73.1, 117.5, 126.4, 129.3, 138.1, 138.3, 139.6, 150.1. HR-ESI-TOF MS ($m/z$): Found 403.0793[M+Na]$^+$ (Calcd 403.0797 for [$C_{22}H_{20}O_2S_2Na$]$^+$). Anal. Calcd for $C_{22}H_{20}O_2S_2$: C, 69.44; H, 5.30. Found: C, 69.46; H, 5.32.

**2-(Mesityl(1H-pyrrole-2-yl) methyl)thieno[3, 2-*b*]thiophene-5-yl)methyl)-1H-pyrrole (4).**

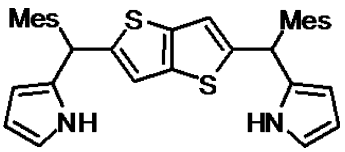

Compound **2** (1g, 2.29 mmol) was dissolved in pyrrole (15 mL, 0.19 mol). The solution was stirred for 45 min under nitrogen atmosphere at room temperature. Trifluoroacetic acid (0.05 mL, 0.22 mmol) was added and stirred for 1 h. The reaction mixture was quenched by dichloromethane; product was neutralized by NaOH (aq) solution, extracted by dichloromethane, dried over $Na_2SO_4$, and dried in rotary evaporator to give yellow oil. The crude product was purified by silica gel chromatography using 10% ethyl acetate−hexane mixture. Compound **4** was obtained as light yellow foam. Yield 0.702 g (57%). $^1$H NMR (500 MHz, $CDCl_3$, 300 K, $\delta$ [ppm]): 2.03 (s, 6H, -Me); 2.29−2.35 (s, 12H, -Me); 4.24 (s, 2H,-CH); 6.03 (br, 1H, $\beta$-H of pyrrole); 6.13 (s, 1H, $\beta$-H of thienothiophene); 6.23 (d, 1H, J = 4.5 Hz, $\beta$-H of pyrrole); 6.30 (d, 1H, J = 4.5 Hz, $\beta$-H of pyrrole); 6.54 (br, 1H, $\beta$-H of pyrrole); 6.69 (s, 1H, $\beta$-H of thienothiophene); 6.70−6.71 (m, 1H, $\beta$-H of pyrrole), 6.72−6.73 (m, 1H, $\beta$-H of pyrrole); 6.86 (s, 2H, Mesityl-CH); 6.92 (s, 2H, Mesityl-CH); 7.99 (br, 1H, -NH); 8.50 (br, 1H, -NH). $^{13}$CNMR (125 MHz, $CDCl_3$, 300 K, $\delta$ [ppm]): 20.1, 20.7, 20.9, 21.1, 30.8, 41.2, 107.4, 108.5, 109.2, 109.4, 117.0, 117.4, 118.9, 124.7, 126.3, 129.2, 130.6, 133.3, 134.0, 135.9,


DOI: 10.1021/acs.joc.6b02576
J. Org. Chem. 2017, 82, 556−566

136.4, 136.5, 136.8, 137.0, 137.1, 137.2, 137.5, 145.5. HR-ESI-TOF MS ($m/z$): Found 534.2145 [$M^+$] (Calcd 534.2163 for [$C_{34}H_{34}N_2S_2]^+$). Anal. Calcd for $C_{34}H_{34}N_2S_2$: C, 76.36; H, 6.41, N, 5.24. Found: C, 76.39; H, 6.45; N, 5.20.

**2-(Tolyl(1H-pyrrole-2-yl) methyl)thieno[3, 2-*b*]thiophene-5-yl)methyl)-1H-pyrrole (5).**

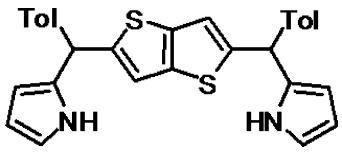


Following the synthetic procedure described for **4**, **5** was obtained starting from **3**. Yield 0.895 g (81%). $^1$H NMR (500 MHz, $CDCl_3$, 300 K, $\delta$ [ppm]): 2. 38 (s, 6H, -Me); 5.63 (s, 2H, −CH); 5.97 (br, 2H, $\beta$-H of pyrrole); 6.86 (s, 2H, $\beta$-H of thienothiophene); 6.69 (d, 2H, J = 4.5 Hz, $\beta$-H of pyrrole); 6.70 (d, 2H, J = 4.5 Hz, $\beta$-H of pyrrole); 7.16 (d, 4H, J = 10 Hz, CH−Tolyl); 7.12 (d, 4H, J = 10 Hz, CH−Tolyl); 7.91 (br, 2H, -NH). $^{13}$CNMR (125 MHz, $CDCl_3$, 300 K, $\delta$ [ppm]): 21.2, 46.5, 107.8, 108.6, 117.3, 118.4, 128.4, 129.4, 132.9, 137.0, 137.8, 139.5, 148.7. HR-ESI-TOF MS ($m/z$): Found 478.1567 [$M^+$] (Calcd 478.1537 for [$C_{30}H_{26}N_2S_2]^+$). Anal. Calcd for $C_{30}H_{26}N_2S_2$: C, 75.28; H, 5.47; N, 5.85. Found: C, 75.29; H, 5.49; N, 5.84.

**General Synthetic Procedure of Compound 6-$H_2$.** Under nitrogen atmosphere and in dark condition a solution of 534 mg of compound **4** (1 mmol) and pentafluorobenzaldehyde (0.12 mL, 1 mmol) in 250 mL dry dichloromethane was stirred for 30 min. Afterward, catalytic amount of p-TSA (95 mg) was added to the reaction mixture and stirred at RT for 90 min. Then chloranil (490 mg, 1.99 mmol) was added and opened to air and the mixture was refluxed for another 1 h. The solvent was removed under reduced pressure and compound was filtered by basic alumina followed by repeated silica gel column chromatography with the mixture of 40% dichloromethane−hexane solution. After recrystallization, the title compound was yielded as dark red crystal.Yield. ~ 85 mg (~6%). mp > 350 °C. MALDI-TOF MS ($m/z$): Found 1416.3415 (Calcd 1416.3385 for [$C_{82}H_{58}F_{10}N_4S_4]^+$). UV−vis ($CH_2Cl_2$, $\lambda$ [nm], ($\epsilon$ [$M^{-1}$ $cm^{-1}$×$10^3$]), 298 K): 517(43.79); 658 (8.56). Anal. Calcd for $C_{82}H_{58}F_{10}N_4S_4$: C, 69.47; H, 4.12; N, 3.95. Found: C, 69.48; H, 4.15; N, 3.93. $^1$H NMR (600 MHz, $CD_2Cl_2$, 193 K, $\delta$ [ppm], TMS): 1.45 (s, *exo-o*-Mes), 2.41 (s, *p*-$CH_3$); 3.27 (s, endo- *o*-Mes); 5.81 (brs, pyrrole $\beta$-H); 6.62 (brs, pyrrole $\beta$-H) ;6,87 (brs, *exo-m*-Mes); 7.20 (s, −CH TT); 7.47 (brs, *endo-m*-Mes)); 9.96 (s, TT $\beta$-H < 96>); 17.75 (brs, s, < 0 > NH); 18.61 (s, < 96 > NH). $^1$H NMR (600 MHz, 1% $CF_3COOH/CD_2Cl_2$, 273 K, $\delta$ [ppm], TMS): 1.70 (s, *o*-$CH_3$); 1.81 (s, *p*-$CH_3$); 1.86 (s, *p*-$CH_3$); 2.04 (s, *o*-$CH_3$); 3.78 (d, J = 3.5, 1H, pyrrole $\beta$-H) ; 3.88 (d, J = 4.2, 1H, pyrrole $\beta$-H); 6.29 (s, −CH mesityl); 6.39 (s, −CH mesityl); 6.94 (s, TT $\beta$-H); 16.37 (brs, pyrrole $\beta$-H); 16.90 (brs, pyrrole $\beta$-H); 17.21 (s, TT $\beta$-H); 22.52 (s, -NH).

**General Synthetic Procedure of Compound 7-$H_2$.** Under nitrogen atmosphere and in dark condition a solution of 478 mg of compound **5** (1 mmol) and pentafluorobenzaldehyde (0.12 mL, 1 mmol) in 250 mL dry dichloromethane was stirred for 30 min. Afterward, catalytic amount of *p*-TSA (95 mg) was added to the reaction mixture and stirred at RT for 90 min. Then chloranil (490 mg, 1.99 mmol) was added and opened to air and the mixture was refluxed for another 1 h. The solvent was removed under reduced pressure and compound was filtered by basic alumina followed by repeated silica gel column chromatography with the mixture of 40% dichloromethane−hexane solution. After recrystallization, the title compound was yielded as dark red crystal. Yield. ~ 110 mg (~8%). m.p > 350 °C. MALDI -TOF MS ($m/z$): Found 1304.2170 (Calc. 1304.2133 for [$C_{74}H_{42}N_4F_{10}S_4]^+$). UV−vis ($CH_2Cl_2$, $\lambda$ [nm], ($\epsilon$ [$M^{-1}$ $cm^{-1}$×$10^3$]), 298 K): 511(50.65); 683 (8.15). Anal. Calcd for $C_{74}H_{42}N_4F_{10}S_4$: C, 68.09; H, 3.24; N, 4.29. Found: C, 68.11; H, 3.25; N, 4.27. $^1$H NMR (600 MHz, $CD_2Cl_2$, 213 K, $\delta$ [ppm], TMS): 2.46−2.52 (s, *p*-$CH_3$); 6.04 (d, pyrrole $\beta$-H); 6.30 (d, pyrrole $\beta$-H); 7.28−7.37 (Tol-CHs); 7.81 (s, −CH TT); 9.98 (s, TT $\beta$-H < 96>); 17.50 (brs, s, < 0 > NH); 17.98 (s, < 96 > NH). $^1$H NMR (500 MHz, 1% $CF_3COOH/CDCl_3$, 288 K, $\delta$ [ppm], TMS): 2.24 (s, 6H, *p*-$CH_3$); 2.28 (s,6H, *p* −$CH_3$); 5.22 (d, J = 4.5, 2H, pyrrole $\beta$-H); 5.64 (d, 2H, J = 5, pyrrole $\beta$-H) ;6.08 (s, 2H, TT $\beta$-H); 6.50 (d, 4H, J = 7.5, Tolyl-H); 6.74 (d, 4H, J = 8, Tolyl-CH); 6.89 (d, 4H, J = 8, Tolyl-CH); 7.00 (d, 4H, J = 8, Tolyl-CH); 12.78 (s, 2H, pyrrole $\beta$-H); 13.11 (s, 2H, pyrrole $\beta$-H); 13.15 (s, 2H, TT $\beta$-H); 17.38 (brs, 2H, pyrrole -NH).

## ■ ASSOCIATED CONTENT

### Supporting Information

The Supporting Information is available free of charge on the ACS Publications website at DOI: 10.1021/acs.joc.6b02576.

X-ray crystallographic data for **6**-$H_2$(CIF)
X-ray crystallographic data for **6**-$H_4^+$ (CIF)
X-ray crystallographic data for **7**-$H_2$(CIF)
Jmol files (ZIP)
Scheme, HR-ESI-TOF mass spectra, MALDI-TOF mass spectra, NMR spectra ($^1$H NMR, $^{13}$C NMR, acid titration, variable temperature, $^1$H−$^1$H COSY, $^1$H−$^1$H ROESY, $^1$H−$^1$H NOESY), details of absorption spectroscopic (solvent dependent, acid titration, variable temperature study), results of DFT calculations, TA spectra, and Cartesian coordinates (PDF)

## ■ AUTHOR INFORMATION

### Corresponding Authors

*marcin.stepien@chem.uni.wroc.pl
*dongho@yonsei.ac.kr
*ichr@iacs.res.in

### ORCID

Dongho Kim: 0000-0001-8668-2644
Harapriya Rath: 0000-0002-5507-5275

### Author Contributions

⊥A.M. and J.O. contributed equally to this work.

### Notes

The authors declare no competing financial interest.

## ■ ACKNOWLEDGMENTS

The work at IACS, Kolkata was supported by DST-SERB (SR/S1/IC-37/2012) and DST-SERB Ramanujan Fellowship (SR/S2/RJN-93/2011), India. A.M. thanks CSIR for senior research fellowship. The work at Yonsei University was supported by the Global Research Laboratory Program (2013K1A1A2A02050183) funded by the Ministry of Science, ICT & Future, Korea. Financial support from the National Science Center of Poland (grant 2014/13/B/ST5/04394 to M.S.) is gratefully acknowledged. Quantum chemical calculations were performed in the Centers for Networking and Supercomputing of Wrocław and Poznań.We are indebted to the Single Crystal X-ray Diffractometer facility in NISER, Bhubaneswar, Odisha, India. We sincerely thank Dr. Palani Sasikumar, Presidency University, Kolkata, India for final refinement of crystal data reported in this manuscript.

## ■ REFERENCES

(1) Turro, N. J. *Angew. Chem., Int. Ed. Engl.* **1986**, *25*, 882.
(2) (a) Rzepa, H. S. *Chem. Rev.* **2005**, *105*, 3697. (b) Herges, R. *Chem. Rev.* **2006**, *106*, 4820. (c) Heilbronner, E. *Tetrahedron Lett.* **1964**, *5*, 1923. (d) Ajami, D.; Oeckler, O.; Simon, A.; Herges, R.


DOI: 10.1021/acs.joc.6b02576
J. Org. Chem. 2017, 82, 556−566

*Nature* **2003**, *426*, 819. (e) Schaller, G. R.; Topić, F.; Rissanen, K.; Okamoto, Y.; Shen, J.; Herges, R. *Nat. Chem.* **2014**, *6*, 608.
(3) (a) Sessler, J. L.; Weghorn, S. J. *Expanded, Contracted and Isomeric Porphyrins*; Pergamon: New York, 1997; Vol. *15*, p 429. (b) Chandrashekar, T. K.; Venkatraman, S. *Acc. Chem. Res.* **2003**, *36*, 676. (c) Sessler, J. L.; Seidel, D. *Angew. Chem., Int. Ed.* **2003**, *42*, 5134. (d) Saito, S.; Osuka, A. *Angew. Chem., Int. Ed.* **2011**, *50*, 4342. (e) Stępień, M.; Sprutta, N.; Latos-Grażyński, L. *Angew. Chem., Int. Ed.* **2011**, *50*, 4288. (f) Sung, Y. M.; Yoon, M.-C.; Lim, J. M.; Rath, H.; Naoda, K.; Osuka, A.; Kim, D. *Nat. Chem.* **2015**, *7*, 418. (g) Oh, J.; Mori, H.; Sung, Y. M.; Kim, W.; Osuka, A.; Kim, D. *Chem. Sci.* **2016**, *7*, 2239.
(4) (a) Stępień, M.; Sprutta, N.; Chwalisz, P.; Szterenberg, L.; Latos-Grażyński, L. *Angew. Chem., Int. Ed.* **2007**, *46*, 7869. (b) Stępień, M.; Szyszko, B.; Latos-Grażyński, L. *J. Am. Chem. Soc.* **2010**, *132*, 3140. (c) Rappaport, S. M.; Rzepa, H. S. *J. Am. Chem. Soc.* **2008**, *130*, 7613. (d) Szyszko, B.; Sprutta, N.; Chwalisz, P.; Stępień, M.; Latos-Grażyński, L. *Chem. - Eur. J.* **2014**, *20*, 1985. (e) Yoon, Z. S.; Osuka, A.; Kim, D. *Nat. Chem.* **2009**, *1*, 113. and references therein. (f) Möbius, K.; Plato, M.; Klihm, G.; Laurich, C.; Savitsky, A.; Lubitz, W.; Szyszko, B.; Stępień, M.; Latos-Grazynski, L. *Phys. Chem. Chem. Phys.* **2015**, *17*, 6644. (g) Cha, W. − Y.; Soya, T.; Tanaka, T.; Mori, H.; Hong, Y.; Lee, S.; Park, K. H.; Osuka, A.; Kim, D. *Chem. Commun.* **2016**, *52*, 6076. (h) Mallick, A.; Rath, H. *Chem. - Asian J.* **2016**, *11* (7), 986. (i) Ghosh, A.; Chaudhary, A.; Srinivasan, A.; Suresh, C. H.; Chandrashekar, T. K. *Chem. - Eur. J.* **2016**, *22*, 3942.
(5) (a) Lim, J. M.; Shin, J.-Y.; Tanaka, Y.; Saito, S.; Osuka, A.; Kim, D. *J. Am. Chem. Soc.* **2010**, *132* (9), 3105. (b) Saito, S.; Shin, J.-Y.; Lim, J. M.; Kim, K. S.; Kim, D.; Osuka, A. *Angew. Chem., Int. Ed.* **2008**, *47*, 9657. (c) Kido, H.; Shin, J.-Y.; Shinokubo, H. *Angew. Chem., Int. Ed.* **2013**, *52*, 13727. (d) Tanaka, Y.; Saito, S.; Mori, S.; Aratani, N.; Shinokubo, H.; Shibata, N.; Higuchi, Y.; Yoon, Z. S.; Kim, K. S.; Noh, S. B.; Park, J. K.; Kim, D.; Osuka, A. *Angew. Chem., Int. Ed.* **2008**, *47*, 681. (e) Alonso, M.; Pinter, B.; Geerlings, P.; De Proft, F. *Chem. - Eur. J.* **2015**, *21*, 17631. (f) Yoon, M.-C.; Shin, J.-Y.; Lim, J. M.; Saito, S.; Yoneda, T.; Osuka, A.; Kim, D. *Chem. - Eur. J.* **2011**, *17*, 6707. (g) Alonso, M.; Geerlings, P.; de Proft, F. *Chem. - Eur. J.* **2012**, *18*, 10916.
(6) (a) Karthik, G.; Lim, J. M.; Srinivasan, A.; Suresh, C. H.; Kim, D.; Chandrashekar, T. K. *Chem. - Eur. J.* **2013**, *19*, 17011. (b) Rath, H.; Sankar, J.; Prabhuraja, V.; Chandrashekar, T. K.; Joshi, B. S.; Roy, R. *Chem. Commun.* **2005**, 3343.
(7) Fuller, L. S.; Iddon, B.; Smith, K. M. *J. Chem. Soc., Perkin Trans. 1* **1997**, *22*, 3465.
(8) Setsune, J.-I.; Katakami, Y.; Iizuna, N. *J. Am. Chem. Soc.* **1999**, *121*, 8957.
(9) Rath, H.; Mallick, A.; Ghosh, T.; Kalita, A. *Chem. Commun.* **2014**, *50*, 9094.
(10) (a) Yoon, M.-C.; Cho, S.; Suzuki, M.; Osuka, A.; Kim, D. *J. Am. Chem. Soc.* **2009**, *131*, 7360. (b) Oh, J.; Sung, Y. M.; Kim, W.; Mori, S.; Osuka, A.; Kim, D. *Angew. Chem., Int. Ed.* **2016**, *55*, 6487. (c) Shin, J.-Y.; Yoon, M.-C.; Lim, J. M.; Yoon, Z. S.; Osuka, A.; Kim, D.; Kim, K. S. *Chem. Soc. Rev.* **2010**, *39*, 2751.
(11) Frisch, M. J.; Trucks, G. W.; Schlegel, H. B.; Scuseria, G. E.; Robb, M. A.; Cheeseman, J. R.; Scalmani, G.; Barone, V.; Mennucci, B.; Petersson, G. A.; Nakatsuji, H.; Caricato, M.; Li, X.; Hratchian, H. P.; Izmaylov, A. F.; Bloino, J.; Zheng, G.; Sonnenberg, J. L.; Hada, M.; Ehara, M.; Toyota, K.; Fukuda, R.; Hasegawa, J.; Ishida, M.; Nakajima, T.; Honda, Y.; Kitao, O.; Nakai, H.; Vreven, T.; Montgomery, J. A.; Peralta, J. E.; Ogliaro, F.; Bearpark, M.; Heyd, J. J.; Brothers, E.; Kudin, K. N.; Staroverov, V. N.; Kobayashi, R.; Normand, J.; Raghavachari, K.; Rendell, A.; Burant, J. C.; Iyengar, S. S.; Tomasi, J.; Cossi, M.; Rega, N.; Millam, J. M.; Klene, M.; Knox, J. E.; Cross, J. B.; Bakken, V.; Adamo, C.; Jaramillo, J.; Gomperts, R.; Stratmann, R. E.; Yazyev, O.; Austin, A. J.; Cammi, R.; Pomelli, C.; Ochterski, J. W.; Martin, R. L.; Morokuma, K.; Zakrzewski, V. G.; Voth, G. A.; Salvador, P.; Dannenberg, J. J.; Dapprich, S.; Daniels, A. D.; Farkas, Ö.; Foresman, J. B.; Ortiz, J. V.; Cioslowski, J.; Fox, D. J. *Gaussian 09*, Revision E.01; Gaussian, Inc.: Wallingford CT, 2009.
(12) Kang, J. K.; Musgrave, C. B. *J. Chem. Phys.* **2001**, *115*, 11040.


DOI: 10.1021/acs.joc.6b02576
*J. Org. Chem.* 2017, 82, 556−566